Hindawi
International Journal of Photoenergy
Volume 2020, Article ID 8865010, 5 pages
https://doi.org/10.1155/2020/8865010

Research Article

Photovoltaic and Charge Trapping Characteristics of Screen-Printed Monocrystalline Silicon Solar Cells with Molybdenum Oxides as Hole-Selective Layers by H_2/Ar Plasma Pretreatment

Chin-Lung Cheng, Chi-Chung Liu, and Chih-Chieh Hsu

Department of Electro-Optical Engineering, National Formosa University, Yunlin 63201, Taiwan

Correspondence should be addressed to Chin-Lung Cheng; chengcl@nfu.edu.tw

Received 15 August 2020; Accepted 6 November 2020; Published 16 November 2020

Academic Editor: Alberto Álvarez-Gallegos

Photovoltaic characteristics of screen-printed monocrystalline silicon solar cells (SPSSCs) with molybdenum oxide (MoO_x) as hole-selective layers (HSLs) were demonstrated. A H_2/Ar plasma pretreatment (PPT) was incorporated into a MoO_x/p-Si(100) interface, which shows the expected quality in terms of passivation. Moreover, the charge trapping characteristics of the MoO_x/p-Si(100) interface were presented. The PPT parameters, including power, treated time, flow ratio of H_2/Ar, and temperature, were investigated. The experimental results indicate that the Si-H bond with a relatively high intensity was demonstrated for the H_2/Ar PPT. The achievement of a conversion efficiency (CE) improvement of more than 1.2% absolute from 18.3% to 19.5% for SPSSCs with H_2/Ar PPT was explored. The promoted mechanism was attributed to the reduction of the interface trap density caused by the large number of Si-H bonds at the silicon substrate and MoO_x interface.

1. Introduction

Passivated emitter and rear cell (PERC) silicon solar cells are the mainstream of the industrial solar cells today [1–3]. To increase the capture of photons by solar cells, PERC introduces two additional layers at the rear of the cell compared with SPSSCs [4]. The function of those layers is to improve the passivation of the rear side and increase the reflection of the back light [5]. However, PERC still have a small amount of Al back surface field (Al-BSF), which will cause recombination [6]. Thus, to improve this shortcoming, transition metal oxides, such as MoO_2, V_2O_5, and WO_3, are proposed as hole-selective layers (HSLs) [7–10]. The energy band of the p-type silicon substrate was matched with the HSL. Moreover, oxygen vacancy defects in the film can be utilized to transfer holes [11]. Therefore, the laser local opening and Al-BSF can be prevented.

Literatures reported that hydrogen (H_2) PPT in fabricating silicon heterojunction solar cells can be adopted to improve surface atomic hydrogen coverage and avoid the generation of defects on the silicon substrate [12]. The H_2 PPT of the Si surface can lead to improvements in minority carrier lifetime [13]. Moreover, the H_2 PPT improves surface passivation compared to classical HF dip [14]. Furthermore, carbon and oxygen contamination can be removed from silicon surfaces by a 30 s H_2 plasma treatment [15]. Thus, to enhance the interface characteristics of silicon and MoO_x, a H_2/Ar PPT was investigated.

2. Experimental Methods

To demonstrate the effects of H_2/Ar plasma treatment on photovoltaic characterizations of the SPSSCs, square samples ($20 \times 20\,mm^2$) of (100)-oriented p-type silicon wafers with 1–3 Ω cm and $190 \pm 20\,\mu m$ were prepared. The texturing process was performed in a solution of 1.73% KOH at 83°C for 10 min. The front emitters were formed by phosphorus diffusion at 840°C for doping and drive-in. After single-side edge isolation and PSG etching processes, the sheet resistances of the front emitters were demonstrated to be approximately $100 \pm 10\,\Omega$/sq. For antireflection coating, a standard SiN_x film with a thickness of 75 nm was deposited on the

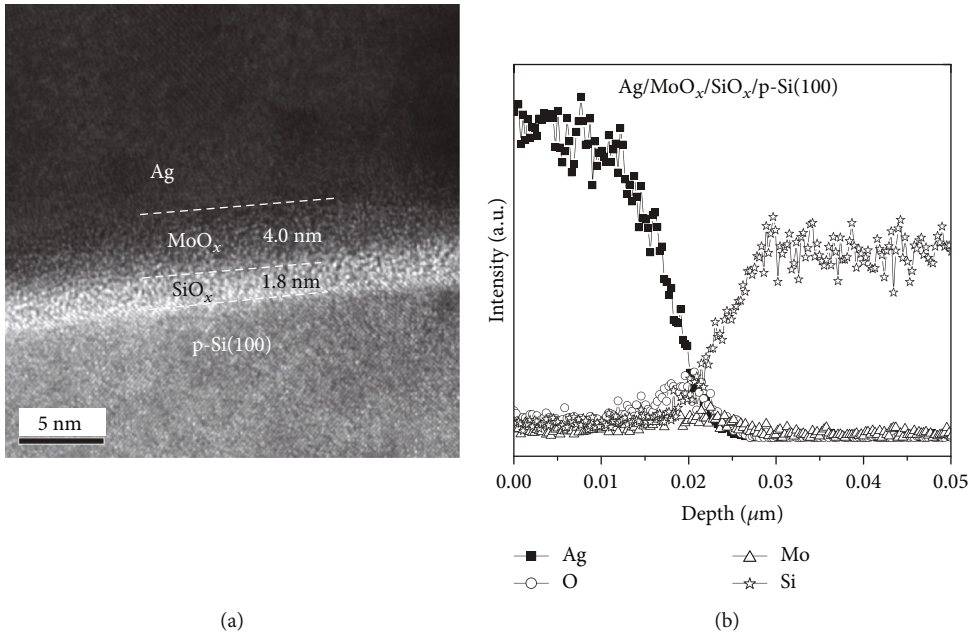

Figure 1: (a) TEM cross-section image and (b) elemental analysis of p-Si(100)/MoO_x/Ag stacked films with H_2/Ar PPT.

n^+-emitters using plasma-enhanced chemical vapor deposition at a frequency of 13.56 MHz. Next, an Ag front paste was screen-printed on the front side of the SPSSCs and dried in an infrared belt furnace at 230°C. Then, a 6-zone industrial infrared belt furnace was utilized to fire Ag pastes into the n-type emitters. The peak temperature and the belt speed were set at 790°C and 508 cm/min, respectively. To protect the front metallization of the SPSSCs, the polymer paste was spin-cast onto the front surface of the SPSSCs at 3000 rpm and dried at 150°C for 30 min. Then, the H_2/Ar PPT was performed on the rear of the cells at power ranged from 50 to 70 W. The treated time was tuned from 0 to 70 s. The $H_2/(H_2 + Ar)$ ratio and temperature were achieved from 22.2 to 66.6% and 200 to 300°C, respectively. The cell without H_2/Ar PPT was presented as a reference. Next, all HSLs consist of MoO_x/Ag films which were achieved by a thermally evaporated technique. Deposition of the approximately 4 nm thick MoO_x films was performed by thermal evaporation from granules of MoO_2 (99.9% purity). The thicknesses of evaporated Ag were 500 nm. The CEs of the SPSSCs were measured under standard test conditions (AM 1.5G spectrum, 100 mW/cm^2, 25°C). The cross-section images and elemental analysis of p-Si(100)/MoO_x/Ag were examined by transmission electron microscopy (TEM) and energy-dispersive X-ray spectroscopy (EDS), respectively. The Si-H bonds of the H_2/Ar PPT samples were measured using Fourier-transform infrared spectroscopy (FTIR).

3. Results and Discussion

The cross-section image and elemental analysis of p-Si(100)/MoO_x/Ag stacked films were examined by the TEM and EDS with a line drawn as shown in Figure 1. The thicknesses of the MoO_x HSLs and SiO_x were demonstrated to be approximately 4 and 1.8 nm, respectively. The SiO_x interfacial layer is present at the MoO_x/Si(100) interface during MoO_x evaporation [16]. Elemental analysis of the p-Si(100)/SiO_x/MoO_x/Ag stacked films by EDS is shown in Figure 1(b). The MoO_x were thermally evaporated at a base pressure of 5×10^{-6} Torr. The Mo/O atomic ratio in the MoO_x layers was approximately 1/2.3 for the MoO_2 source granules. Literature reported that the Mo^{+4}, Mo^{+5}, or Mo^{+6} states could be presented in MoO_x HSL [17]. In this work, the O/Mo atomic ratio of 2.3 in the MoO_x HSLs for the MoO_2 granule source was attributed to some oxygen already being in the chamber during evaporation [16].

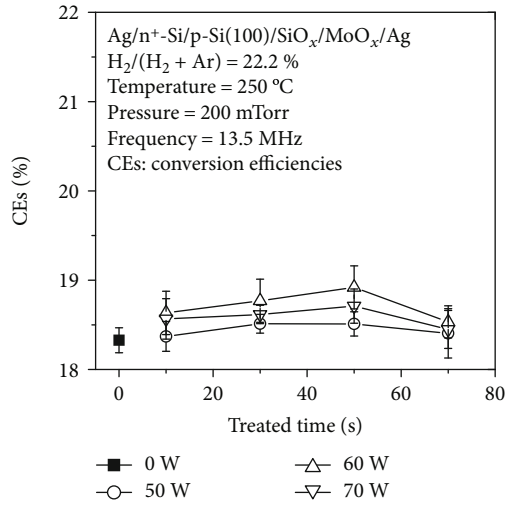

Figure 2: CEs vs. treated time curves of the SPSSCs with and without H_2/Ar PPT. The $H_2/(H_2 + Ar)$ ratio and temperature were achieved at 22.2% and 250°C, respectively.

Figure 2 shows CEs vs. treated time curves of the SPSSCs with and without H_2/Ar PPT. The $H_2/(H_2 + Ar)$ ratio and

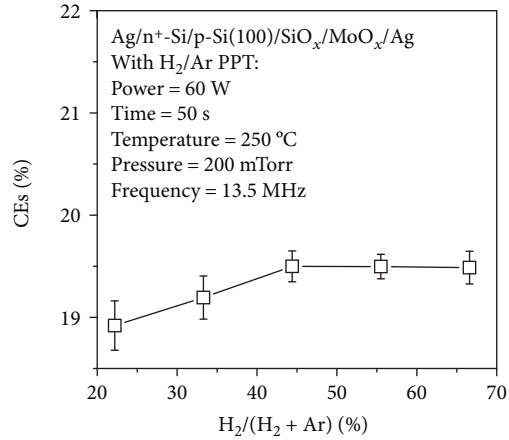

Figure 3: CEs vs. $H_2/(H_2 + Ar)$ ratio curves of the SPSSCs. The treated parameters were addressed at 60 W for 50 s and 250°C.

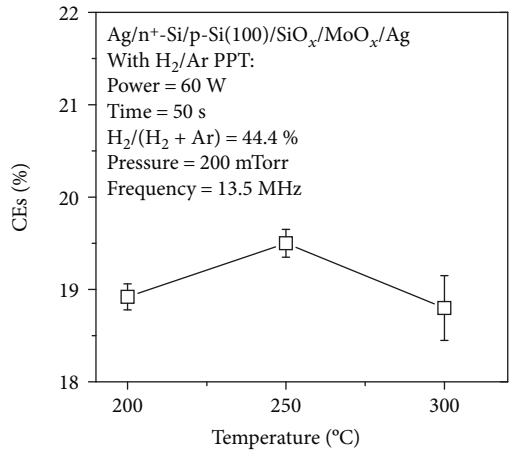

Figure 4: CEs vs. temperature curves of the SPSSCs. The treated parameters were addressed at 60 W for 50 s and $H_2/(H_2 + Ar)$ of 44.4%.

temperature were achieved at 22.2% and 250°C, respectively. The CE was enhanced by increasing the treated time. However, an excess of treated time could cause a degradation of the CE due to the increase of dangling bond defects on the surface, which can result in etching effects of the H_2 plasma [12]. Compared with various powers and treated time, a better CE improvement was demonstrated at a power of 60 W for 50 s. The achievement of a CE improvement of more than 0.6% absolute from 18.3% to 18.9% for SPSSCs with and without H_2/Ar PPT was explored.

To investigate the effects of various $H_2/(H_2 + Ar)$ ratios, the CEs of the SPSSCs are shown in Figure 3. The CE increases as the $H_2/(H_2 + Ar)$ ratio is increased, until an optimum of the $H_2/(H_2 + Ar)$ ratio is reached. Above this optimum condition, the CE decreases as the $H_2/(H_2 + Ar)$ ratio increases. The upgraded mechanism is related to a change in surface hydrogen configuration toward lower hydrides [13]. Excessive H_2/Ar PPT will cause the surface roughness to further degrade the characteristics of the cells [14]. Achieving CE improvement of more than 0.6% absolute from 18.9% to 19.5% for SPSSCs with a tuning $H_2/(H_2 + Ar)$ ratio was explored. Thus, a H_2/Ar PPT was incorporated into a MoO_x/p-Si(100) interface, which shows the expected qualities in terms of passivation.

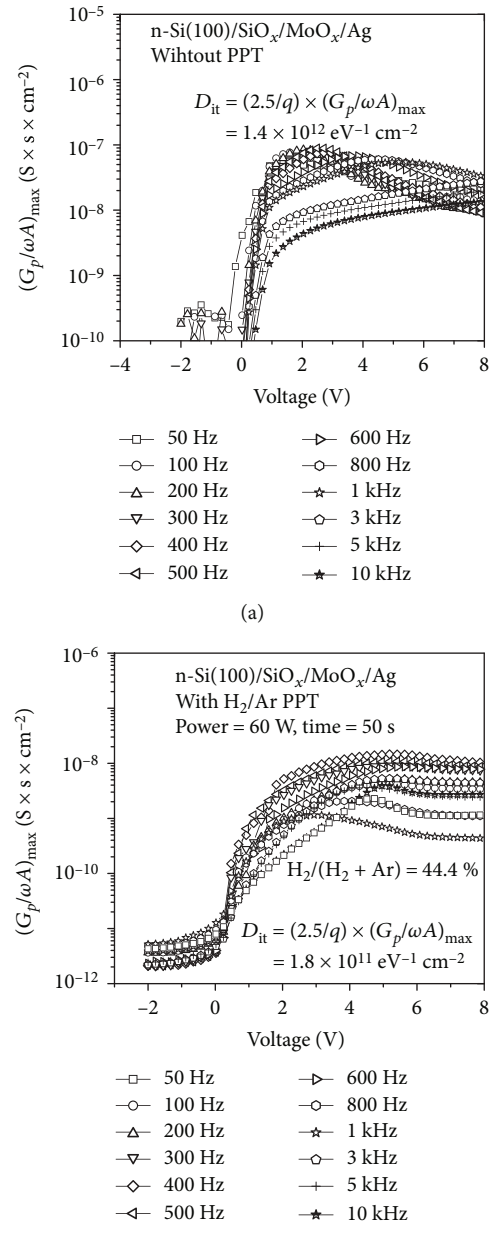

Figure 5: D_{it} of n-Si(100)/SiO_x/MoO_x/Ag capacitors (a) with and (b) without H_2/Ar PPT extracted from the conductance method. The conductance of n-Si(100)/SiO_x/MoO_x/Ag capacitors as a function of frequency was measured and plotted as $G_p/\omega A$ versus voltages by biasing the Si surface in depletion condition.

For further examining the photovoltaic characteristics of the SPSSCs, Figure 4 shows CEs vs. temperature curves of the SPSSCs. As the duration of temperature exposure increased, the CE increased to 250°C and then decreased. The increase in CE due to the PPT is familiarly considered to result from passivation of surface defects. It has been reported that the

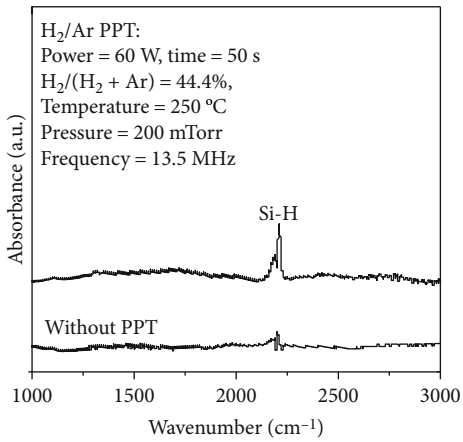

Figure 6: FTIR spectra of silicon substrate with and without H_2/Ar PPT samples at wavenumbers ranging from 1000 to 3500 cm^{-1}.

smaller effective surface recombination velocity can be achieved by the higher deposition temperature [14]. The results indicate that the best result in this work is a CE of 19.5% at deposition temperature ranging from 250 to 300°C.

Because MoO_x/silicon contacts induce slightly Fermi level bending on p-type silicon, the interface characteristics were addressed by a MoO_x/n-type silicon structure [18]. Figure 5 shows the interface trap density (D_{it}) of n-Si(100)/SiO_x/MoO_x/Ag capacitors (a) with and (b) without H_2/Ar PPT extracted from the conductance method. The conductance (G_p) of n-Si(100)/SiO_x/MoO_x/Ag capacitors as a function of frequency (ω) was measured and plotted as $G_p/\omega A$ versus voltages by biasing the Si surface in depletion condition [19]. A was denoted as the area of the capacitor. Figure 5 shows that $G_p/\omega A$ of the cells without H_2/Ar PPT has a maximum value and D_{it} is equal to $(2.5/q)(G_p/\omega A)_{max}$ at that maximum [20]. It is also observed that the D_{it} values of the cells with and without H_2/Ar PPT were 1.8×10^{11} and 1.4×10^{12} eV^{-1} cm^{-2}, respectively. Obviously, a H_2/Ar PPT is beneficial to improve the interface characteristics of MoO_x and silicon. To further understand the improvement mechanism, FTIR spectra were addressed.

Infrared spectra of the cells with and without H_2/Ar PPT were measured using FTIR. The experimental conditions for FTIR were resolution of 1 cm^{-1}, source of Glowbar which can provide FTIR measurement of wavenumbers ranging from 1000 to 3000 cm^{-1}, and detector mercury-cadmium-telluride. Figure 6 illustrates the FTIR spectra of the cells with and without H_2/Ar PPT. The spectra present an absorption peak at 2170 cm^{-1}, which is recognized as the Si-H bonds [21]. The absorbance values for nontreatment samples at 2170 cm^{-1} are smaller than those of the H_2/Ar PPT ones, demonstrating that the amount of Si-H bonds on the silicon surface is increased by PPT in the H_2/Ar atmosphere.

Figure 7(a) indicates dark and illuminated (AM 1.5G) current density vs. voltage curves of the SPSSCs with and without H_2/Ar PPT. A CE of SPSSCs with PPT in H_2/Ar ambient was demonstrated to be around 19.5%. The CE was found to increase after the silicon substrate was exposed

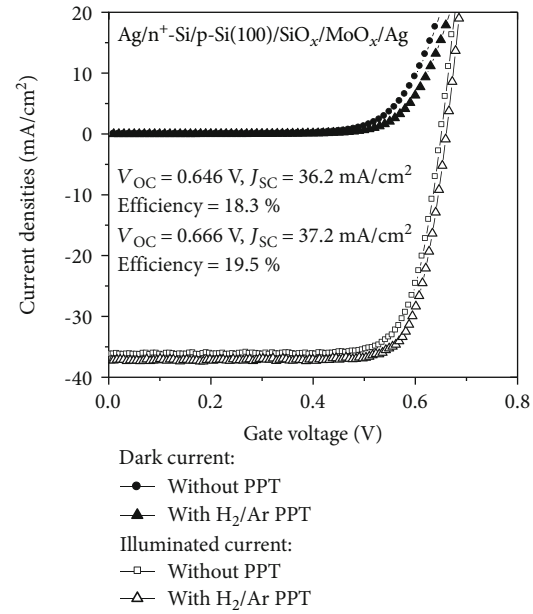

(a)

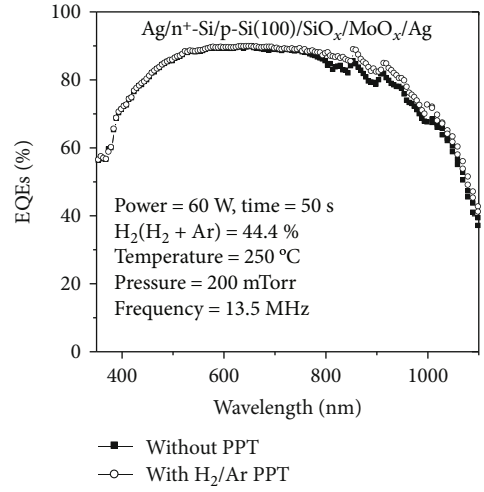

(b)

Figure 7: (a) Dark and illuminated (AM 1.5G) current density vs. voltage curves of the SPSSCs with and without H_2/Ar PPT. (b) EQEs of the SPSSCs with and without H_2/Ar PPT.

to H_2/Ar PPT for 50 s before the evaporation of MoO_x. Moreover, the open-circuit voltages of 666 and 646 mV for SPSSCs with and without H_2/Ar PPT, respectively, were achieved as shown in Figure 7(a). This can be proved by the optimization of the interface trap charge, as shown in Figure 5. To understand the improvement mechanism, external quantum efficiencies (EQEs) of the SPSSCs with and without H_2/Ar PPT are shown in Figure 7(b). Compared without H_2/Ar PPT, an average increase in EQE of around 4.25% was demonstrated for H_2/Ar PPT. In the long wavelength regions, the MoO_x surface passivation strongly improves the EQE. Thus, an increase in the overall EQE was caused by high diffusion length.

4. Conclusions

A H_2/Ar PPT process was applied to monocrystalline silicon substrate before depositing the MoO_x HSLs. The enhanced passivation effects of H_2/Ar PPT were investigated by using a conductance method of measuring D_{it}, in combination with FTIR spectroscopy. The achievement of a CE improvement of more than 1.2% absolute from 18.3% to 19.5% for SPSSCs with H_2/Ar PPT was explored. The promoted mechanism could be attributed to the reduction of D_{it} and the increase of the Si-H bonds at MoO_x and Si substrate.

Data Availability

The data used to support the findings of this study are available from the corresponding author upon request.

Conflicts of Interest

The authors declare that they have no conflicts of interest.

Acknowledgments

The authors would like to thank the Ministry of Science and Technology of the Republic of China for the financial support under Contract No. MOST 108-2221-E-150-009.

References

[1] N. E. Grant, J. R. Scowcroft, A. I. Pointon, M. Al-Amin, P. P. Altermatt, and J. D. Murphy, "Lifetime instabilities in gallium doped monocrystalline PERC silicon solar cells," *Solar Energy Materials and Solar Cells*, vol. 206, article 110299, 2020.

[2] C. B. Mo, S. Park, S. Bae et al., "Minimizing light-induced degradation of the Al2O3Rear passivation layer for highly efficient PERC solar cells," *ECS Journal of Solid State Science Technology*, vol. 7, no. 12, pp. Q253–Q258, 2018.

[3] J. Liu, Y. Yao, S. Xiao, and X. Gu, "Review of status developments of high-efficiency crystalline silicon solar cells," *Journal of Physics D: Applied Physics*, vol. 51, no. 12, p. 123001, 2018.

[4] A. To, W. Min Li, X. Li, and B. Hoex, "The effects of bifacial deposition of ALD AlO_x on the contact properties of screen-printed contacts for p-type PERC solar cells," *Energy Procedia*, vol. 124, pp. 914–921, 2017.

[5] A. Uruena, L. Tous, F. Duerinckx et al., "Understanding the mechanisms of rear reflectance losses in PERC type silicon solar cells," *Energy Procedia*, vol. 38, pp. 801–806, 2013.

[6] J. S. Chiu, Y. M. Zhao, S. Zhang, and D. S. Wuu, "The role of laser ablated backside contact pattern in efficiency improvement of mono crystalline silicon PERC solar cells," *Solar Energy*, vol. 196, pp. 462–467, 2020.

[7] C. W. Chu, S. H. Li, C. W. Chen, V. Shrotriya, and Y. Yang, "High-performance organic thin-film transistors with metal oxide/metal bilayer electrode," *Applied Physics Letters*, vol. 87, no. 19, article 193508, 2005.

[8] L. Fang, S. J. Baik, and K. S. Lim, "Transition metal oxide window layer in thin film amorphous silicon solar cells," *Thin Solid Films*, vol. 556, pp. 515–519, 2014.

[9] L. G. Gerling, S. Mahato, A. Morales-Vilches et al., "Transition metal oxides as hole-selective contacts in silicon heterojunctions solar cells," *Solar Energy Materials and Solar Cells*, vol. 145, pp. 109–115, 2016.

[10] C. L. Cheng, C. C. Liu, Y. S. Chiu, P. W. Chen, and Z. Y. Liu, "Air ambient and composition effects of molybdenum oxides on photovoltaic and physical characteristics of screen-printed mono-crystalline silicon solar cells," *Materials Letters*, vol. 234, pp. 319–322, 2019.

[11] A. L. Fernandes Cauduro, Z. E. Fabrim, M. Ahmadpour et al., "Tuning the optoelectronic properties of amorphous MoOx-films by reactive sputtering," *Applied Physics Letters*, vol. 106, no. 20, article 202101, 2015.

[12] F. Wang, X. Zhang, L. Wang et al., "Role of hydrogen plasma pretreatment in improving passivation of the silicon surface for solar cells applications," *ACS Applied Material Interfaces*, vol. 6, no. 17, pp. 15098–15104, 2014.

[13] S. N. Granata, T. Bearda, F. Dross, I. Gordon, J. Poortmans, and R. Mertens, "Effect of an in-situ H_2 plasma pretreatment on the minority carrier lifetime of a-Si:H(i) passivated crystalline silicon," *Energy Procedia*, vol. 27, pp. 412–418, 2012.

[14] I. Martín, M. Vetter, A. Orpella et al., "Improvement of crystalline silicon surface passivation by hydrogen plasma treatment," *Applied Physics Letters*, vol. 84, no. 9, pp. 1474–1476, 2004.

[15] R. E. Thomas, M. J. Mantini, R. A. Rudder, D. P. Malta, S. V. Hattangady, and R. J. Markunas, "Carbon and oxygen removal from silicon (100) surfaces by remote plasma cleaning techniques," *Journal of Vacuum Science & Technology A: Vacuum, Surfaces, and Films*, vol. 10, no. 4, pp. 817–822, 1992.

[16] C. L. Cheng, C. C. Liu, and Y. W. Shen, "Photovoltaic and charge trapping characteristics of multilayer silver embedded in molybdenum oxides as hole-selective layers for screen-printed monocrystalline silicon solar cell applications," *Journal of Vacuum Science Technology B*, vol. 38, no. 2, article 020602, 2020.

[17] C. T. Lin, C. H. Yeh, M. H. Chen, S. H. Hsu, C. I. Wu, and T. W. Pi, "Influences of evaporation temperature on electronic structures and electrical properties of molybdenum oxide in organic light emitting devices," *Journal Applied Physics*, vol. 107, no. 5, article 053703, 2010.

[18] S. Li, Z. Yao, J. Zhou, R. Zhang, and H. Shen, "Fabrication and characterization of WO_3 thin films on silicon surface by thermal evaporation," *Materials Letters*, vol. 195, pp. 213–216, 2017.

[19] C. L. Cheng, K. S. Chang-Liao, and T. K. Wang, "Improvement on the electrical characteristics of HfO[sub x]N[sub y]-gated metal-oxide-semiconductor devices by high-temperature annealing," *Electrochemical Solid-State Letters*, vol. 9, no. 11, pp. F80–F82, 2006.

[20] E. H. Nicollian and J. R. Brews, *MOS (metal oxide semiconductor) physics and technology*, Wiley, New York, 1982.

[21] K. O. Bugaev, A. A. Zelenina, and V. A. Volodin, "Vibrational spectroscopy of chemical species in silicon and silicon-rich nitride thin films," *International Journal of Spectroscopy*, vol. 2012, Article ID 281851, 5 pages, 2012.